

Modelling the IGM and the $\text{Ly}\alpha$ forest at high redshift from the dark matter distribution

M. Viel ^{1,2,3}, S. Matarrese ¹, H. J. Mo ², Tom Theuns ³ & M. G. Haehnelt ³

¹ *Dipartimento di Fisica ‘Galileo Galilei’, via Marzolo 8, I-35131 Padova, Italy*

² *Max-Planck-Institut für Astrophysik, Karl-Schwarzschild-Strasse 1, D-85741 Garching, Germany*

³ *Institute of Astronomy, Madingley Road, Cambridge CB3 0HA, UK.*

Email: viel@pd.infn.it, matarrese@pd.infn.it, hom@mpa-garching.mpg.de, tt@ast.cam.ac.uk., haehnelt@ast.cam.ac.uk

submitted to MNRAS

ABSTRACT

A variety of approximate schemes for modelling the low-density Intergalactic Medium (IGM) in the high-redshift Universe is compared to the results of a large high-resolution hydro-dynamical simulation. These schemes use either an analytical description of the dark matter distribution and the IGM or numerical simulations of the DM distributions combined with different approximate relations between dark matter field and the gas distribution. Schemes based on a filtering of the dark matter distribution with a global Jeans scale result in a rather poor description of the gas distribution. An adaptive filtering which takes into account the density/temperature dependence of the Jeans scale is required. A reasonable description of the gas distribution can be achieved using a fit of the mean relation between the dark matter and gas densities in the hydro-dynamical simulation to relate dark matter and gas distribution. In the hydro-dynamical simulations deviations from this mean relation are correlated with gradients in the dark matter peculiar velocity field indicative of shocks in the gas component. A scheme which takes into account this correlation results in a further improved gas distribution. Such adaptive filtering schemes applied to dark matter simulations will be very well suited for studies of statistical properties of the $\text{Ly}\alpha$ forest which investigate the IGM and the underlying dark matter distribution and require a large dynamic range and/or an extensive parameter study.

Key words: Cosmology; theory – intergalactic medium – large-scale structure of universe – quasars: absorption lines

1 INTRODUCTION

The low-density Intergalactic Medium (IGM) offers a unique and powerful probe of the high redshift Universe. Numerous weak absorption lines seen in the spectra of distant quasars (the $\text{Ly}\alpha$ forest) are produced by the small residue of neutral hydrogen in filamentary structures intersected by the line of sight (Bahcall & Salpeter 1965; Gunn & Peterson 1965; see Rauch 1998 for a recent review). Such structures arise naturally in hierarchical cold dark matter dominated models of structure formation, in which the IGM is highly ionised by the UV-background produced by stars and galaxies. Simulations show that the low-column density ($N_{\text{HI}} \leq 10^{14.5} \text{ cm}^{-2}$) absorption lines are produced by small fluctuations in the warm ($T \sim 10^4 \text{ K}$) photo-heated IGM, which smoothly traces the mildly non-linear dark matter filaments and sheets on scales larger the Jeans scale

(Cen *et al.* 1994, Petitjean *et al.* 1995, Miralda-Escudé *et al.* 1996, Zhang *et al.* 1998).

This picture is supported by analytical studies based on simple models for the IGM dynamics. Such models are based on either a local non-linear mapping of the linear density contrast, obtained for example by applying a lognormal transformation (Coles & Jones 1991) to the IGM (Bi, Börner & Chu 1992; Bi 1993; Bi, Ge & Fang 1995; Bi & Davidsen 1997, hereafter BD97), or on suitable modifications of the Zel’dovich approximation (Zel’dovich 1970), to account for the smoothing caused by the gas pressure on the Jeans scale (Reisenegger & Miralda-Escudé 1995; Gnedin & Hui 1998; Hui, Gnedin & Zhang 1997; Matarrese & Mohayaee 2002). Many properties of the $\text{Ly}\alpha$ absorbers can be understood with straightforward physical arguments (Schaye 2001).

The most convincing support for this picture comes, however, from the comparison of observed spectra with mock spectra computed from hydrodynamical numerical simulations (Cen *et al.* 1994; Zhang, Anninos & Norman 1995, 1997; Miralda-Escudé *et al.* 1996; Hernquist *et al.* 1996; Charlton *et al.* 1997; Theuns *et al.* 1998). These simulated spectra accurately reproduce many observed properties of the Ly α forest. Although there are still some discrepancies between observed and simulated spectra, especially in the Doppler parameters of the absorption lines (Theuns *et al.* 1998; Bryan *et al.* 1999; Meiksin *et al.* 2001).

Observationally, the unprecedented high resolution observations of the HIRES and UVES spectrographs on the Keck and VLT telescopes, as well as observations with the Hubble Space Telescope, have lead to great advances in the understanding of the Ly α forest. HIRES allowed to detect lines with column densities as low as $N_{\text{HI}} \sim 10^{12} \text{ cm}^{-2}$, while HST made a detailed analysis of the low-redshift Ly α forest at $z < 1.6$ possible. Recent results include limits on the baryon density (Rauch *et al.* 1997), the temperature and equation of state of the IGM (Schaye *et al.* 2000; Theuns *et al.* 2001; Ricotti, Gnedin & Shull 2000; Bryan & Machacek 2000, McDonald *et al.* 2001), the power spectrum of the density fluctuations (Croft *et al.* 1998, 2001, Gnedin & Hamilton 2001, Zaldarriaga *et al.* 2001), the geometry of the Universe (Hui *et al.* 1999; McDonald *et al.* 2001; Viel *et al.* 2002) and direct inversions of the density field (Nusser & Haehnelt 1999, 2000; Pichon *et al.* 2001). Kim *et al.* (2001) used high resolution VLT/UVES data, to make an extensive analysis of the Ly α forest in the redshift range $1.5 < z < 4$. Dobrzycki *et al.* (2001) presented results on the clustering and evolution of the lines at $z < 1.7$ using the HST/FOS spectrograph.

Many aspects of the warm photo-ionised Intergalactic medium can be well modelled by hydrodynamical simulations. Hydro simulations are, however, still rather limited in dynamic range. The box size of hydro simulations which resolve the Jeans mass of the photo-ionised IGM with a temperature of $\sim 10^4 \text{ K}$ probe the large scale fluctuations of the density field rather poorly. This leads to uncertainties due to cosmic variance in the fluctuations on scales approaching the box size and missing fluctuations on scales larger than the simulation box. Because of limited computational resources it is also hardly possible to perform extensive parameter studies. In order to overcome these problems approximate methods for simulating the Ly α forest in QSO absorption spectra are often used (e.g. Gnedin & Hui 1998; Croft *et al.* 1998; Croft *et al.* 1999). We test here a wide range of such approximate methods against a large high-resolution hydro-dynamical simulation.

The plan of the paper is as follows. In Section 2 we briefly describe the hydro-simulation used. Section 3 presents the lognormal model for the IGM and an improved model based on the implementation of the gas probability distribution function taken from the hydro-simulation. We improve our modelling in Section 4, using two different ways of filtering the linear dark matter density field to model pressure effects. In this Section we present a further improvement, based on modelling

the gas distribution starting from the non-linear dark matter density field obtained from the hydro-simulation and we show how the smoothing on the Jeans length of the evolved dark-matter density field poorly reproduces the real gas distribution. In Section 5 we compare the different methods proposed in terms of the 1-point and 2-points PDF of the flux. Section 6 contains a general discussion and our conclusions.

2 THE HYDRO-DYNAMICAL SIMULATION

In the following Sections we will test our approximate schemes to model the Ly α forest against a large high-resolution hydro-dynamical simulation. We therefore summarise here some parameters of the hydro-dynamical simulation used. The simulation techniques are described in more detail in Theuns *et al.* (1998). We analyse a total of 7 outputs at redshifts $z = 49$, $z = 10$, $z = 4$, $z = 3.5$, $z = 3$, $z = 2.25$, $z = 2$ of a periodic, cubic region in a Λ CDM Universe. The cosmological parameters are: $\Omega_{0m} = 0.3$, $\Omega_{0\Lambda} = 0.7$, $H_0 = 100h \text{ km s}^{-1} \text{ Mpc}$ with $h = 0.65$ and $\Omega_{0b}h^2 = 0.019$. The comoving size of the box is $12.0/h \text{ Mpc}$. There are 256^3 DM particles and 256^3 gas particles, whose masses are $m_{\text{DM}} = 1.13 \times 10^7 M_{\odot}$ and $m_{\text{IGM}} = 1.91 \times 10^6 M_{\odot}$. The input linear power spectrum was computed with CMBFAST (Seljak & Zaldarriaga 1996), and normalised to the abundance of galaxy clusters using $\sigma_8 = 0.9$ (Eke, Cole & Frenk 1996), where σ_8 denotes the mass fluctuations in spheres of radius $8h^{-1} \text{ Mpc}$.

The simulation code is based on HYDRA (Couchman *et al.* 1995) and combines Smoothed Particle Hydrodynamics (see *e.g.* Monaghan 1992) with P3M for self-gravity. Spline interpolation over gas particles allows the computation of smooth estimates for density, temperature and velocity and their gradients. The width of the spline kernel is matched to the local particle number density, in this way high density regions have higher numerical resolution than lower density ones. Photo-ionisation and photo-heating rates are computed using the fits in Theuns *et al.* (1998).

Along many randomly chosen sight lines parallel to one of the axis of the simulation box, we compute the gas and DM (over) density and peculiar velocity, the gas temperature, and the neutral hydrogen (density weighted) density, temperature and peculiar velocity. This allows us to compute the absorption spectra. The smooth estimate for the dark matter fields are computed using SPH interpolation as well, with a smoothing length chosen to given of order ~ 32 neighbour contributions per particle (Appendix A).

3 MODELS USING ANALYTIC DESCRIPTIONS OF THE DARK MATTER DISTRIBUTION

3.1 The lognormal model

We have started with the model introduced by Bi and collaborators (Bi *et al.* 1992, 1995; Bi 1993; BD97) for

generating a Ly α absorption spectrum along a LOS. This simple model predicts many properties of the absorption lines, including the column density distribution and the distribution of line widths (b parameters), which can be directly compared with observations (BD97). Recently, the BD97 model has been used by Roy Choudhury *et al.* (2000, 2001) to study neutral hydrogen correlation functions along and transverse to the line-of-sight. Feng & Fang (2000) adopted the BD97 method to analyse non-Gaussian effects on the transmitted flux stressing their importance for the reconstruction of the initial mass density field. Viel *et al.* (2002) implemented a variant of the BD97 model to simulate multiple systems of QSOs and found correlations in the transverse direction in agreement with observations (see also Petry *et al.* 2002 for an analysis of the correlations in the transverse direction).

The BD97 model is based on the assumption that the low-column density Ly α forest is produced by smooth fluctuations in the intergalactic medium which arise as a result of gravitational growth of perturbations. Since the fluctuations are only mildly non-linear, density perturbations in the intergalactic medium $\delta_0^{\text{IGM}}(\mathbf{x}, z)$ can be related to the underlying DM perturbations by a convolution, which models the effects of gas pressure. In Fourier space one has:

$$\delta_0^{\text{IGM}}(\mathbf{k}, z) = W_{\text{IGM}}(k, z) D_+(z) \delta_0^{\text{DM}}(\mathbf{k}) \quad (1)$$

where $D_+(z)$ is the growing mode of density perturbations (normalised so that $D_+(0) = 1$) and $\delta_0^{\text{DM}}(\mathbf{k})$ is the Fourier transformed DM linear over density at $z = 0$. The low-pass filter $W_{\text{IGM}}(k, z) = (1 + k^2/k_J^2)^{-1}$ depends on the comoving Jeans length

$$k_J^{-1}(z) \equiv H_0^{-1} \left[\frac{2\gamma k_B T_m(z)}{3\mu m_p \Omega_{0m}(1+z)} \right]^{1/2}, \quad (2)$$

where k_B is Boltzmann's constant, T_m the gas temperature, μ the molecular weight and γ the ratio of specific heats. Ω_{0m} is the present-day matter density. The Jeans length depends on density and temperature. Jeans smoothing is therefore an adaptive smoothing of the density field. However, for simplicity in most practical implementations the comoving Jeans length is assumed to be constant and computed for the mean density and the mean temperature T_0 at mean density $\delta = 0$. As we will see later this is a severe restriction which significantly affects the results.

Gnedin & Hui (1998) adopt a different and more accurate expression for the IGM filter $W_{\text{IGM}}(k, z)$, which, however, does not allow a simple matching with the non-linear regime (see also the discussion in Section 4.1). More accurate window-functions have also been proposed by Nusser (2000) and Matarrese & Mohayaee (2002). In what follows, we take $T_0(z) \propto 1 + z$, which leads to a constant comoving Jeans scale. This assumption should not be critical as the redshift intervals considered here are small.

Bi & Davidsen adopt a simple lognormal (LN) transformation (Coles & Jones 1991) to obtain the IGM density in the mildly non-linear regime from the linear density field,

$$1 + \delta_{\text{IGM}}(\mathbf{x}, z) = \exp \left[\delta_0^{\text{IGM}}(\mathbf{x}, z) - \frac{\langle (\delta_0^{\text{IGM}})^2 \rangle D_+^2(z)}{2} \right] \quad (3)$$

where $1 + \delta_{\text{IGM}}(\mathbf{x}, z) = n_{\text{IGM}}(\mathbf{x}, z)/\bar{n}_{\text{IGM}}(z)$ and $\bar{n}_{\text{IGM}}(z) \approx 1.12 \times 10^{-5} \Omega_{0b} h^2 (1+z)^3 \text{ cm}^{-3}$. The IGM peculiar velocity \mathbf{v}^{IGM} is related to the linear IGM density contrast via the continuity equation. As in BD97, we assume that the peculiar velocity is still linear even on scales where the density contrast gets non-linear; this yields

$$\mathbf{v}^{\text{IGM}}(\mathbf{k}, z) = E_+(z) \frac{i\mathbf{k}}{k^2} W_{\text{IGM}}(k, z) \delta_0^{\text{DM}}(\mathbf{k}) \quad (4)$$

with $E_+(z) = H(z) f(\Omega_m, \Omega_\Lambda) D_+(z)/(1+z)$. Here $f(\Omega_m, \Omega_\Lambda) \equiv -d \ln D_+(z)/d \ln(1+z)$ (e.g. Lahav *et al.* 1991, for its explicit and general expression) and $H(z)$ is the Hubble parameter at redshift z ,

$$H(z) = H_0 \sqrt{\Omega_{0m}(1+z)^3 + \Omega_{0\mathcal{R}}(1+z)^2 + \Omega_{0\Lambda}} \quad (5)$$

where $\Omega_{0\Lambda}$ is the vacuum-energy contribution to the cosmic density and $\Omega_{0\mathcal{R}} = 1 - \Omega_{0m} - \Omega_{0\Lambda}$ ($\Omega_{0\mathcal{R}} = 0$ for a flat universe). The procedure to obtain 1D LOS random fields from 3D random fields is described in BD97 and Viel *et al.* (2002). We will explore below a more accurate mapping between the linear and non-linear gas density which uses the PDF of the gas density obtained from hydro-dynamical simulations.

The neutral hydrogen density can be computed from the total density, assuming photo-ionisation and taking the optically thin limit, $n_{\text{HI}}(\mathbf{x}, z) = f_{\text{HI}}(T, \Gamma, Y) n_{\text{H}}(\mathbf{x}, z)$, where $n_{\text{H}} = (1 - Y) n_{\text{IGM}}$ and Y is the helium abundance by mass. The photo-ionisation rate $\Gamma \equiv \Gamma_{12} \times 10^{-12} \text{ s}^{-1}$ is related to the spectrum of ionising photons as $\Gamma = \int_{\nu_{\text{th}}}^{\infty} 4\pi J(\nu)/h_P \nu \sigma(\nu) d\nu$, where $\sigma(\nu)$ is the photo-ionisation cross-section and $h_P \nu_{\text{th}}$ the hydrogen ionisation threshold (h_P denotes Planck's constant). $J(\nu) = J_{21}(\nu_0/\nu)^m \times 10^{-21} \text{ erg s}^{-1} \text{ Hz}^{-1} \text{ cm}^{-2} \text{ sr}^{-1}$ with ν_{th} the frequency of the HI ionisation threshold, and m is usually assumed to lie between 1.5 and 1.8. In the highly ionised case ($n_{\text{HI}} \ll n_{\text{IGM}}$) of interest here, one can approximate the local density of neutral hydrogen as (e.g. Hui, Gnedin & Zhang 1997)

$$\frac{n_{\text{HI}}(\mathbf{x}, z)}{\bar{n}_{\text{IGM}}(z)} \approx 10^{-5} \left(\frac{\Omega_{0b} h^2}{0.019} \right) \left(\frac{\Gamma_{-12}}{0.5} \right)^{-1} \left(\frac{1+z}{4} \right)^3 \times \left(\frac{T(\mathbf{x}, z)}{10^4 \text{ K}} \right)^{-0.7} (1 + \delta_{\text{IGM}}(\mathbf{x}, z))^2. \quad (6)$$

The temperature of the low-density IGM is determined by the balance between adiabatic cooling and photo-heating by the UV background, which establishes a local power-law relation between temperature and density, $T(\mathbf{x}, z) = T_0(z)(1 + \delta_{\text{IGM}}(\mathbf{x}, z))^{\gamma(z)-1}$, where both the temperature at mean density T_0 and the adiabatic index γ depend on the IGM ionisation history (Meiksin 1994; Miralda-Escudé & Rees 1994; Hui & Gnedin 1997; Schaye *et al.* 2000; Theuns *et al.* 2001).

Given the neutral density, the optical depth in redshift-space at velocity u (in km s^{-1}) is

$$\tau(u) = \frac{\sigma_{0,\alpha\text{C}}}{H(z)} \int_{-\infty}^{\infty} dy n_{\text{HI}}(y) \mathcal{V}[u - y - v_{\parallel}^{\text{IGM}}(y), b(y)] \quad (7)$$

where $\sigma_{0,\alpha} = 4.45 \times 10^{-18} \text{ cm}^2$ is the hydrogen Ly α cross-section, y is the real-space coordinate (in km s^{-1}), \mathcal{V} is the standard Voigt profile normalised in real-space, and $b = (2k_B T/mc^2)^{1/2}$ is the thermal width. Velocity v and redshift z are related through $d\lambda/\lambda = dv/c$, where $\lambda = \lambda_0(1+z)$. For the low column-density systems considered here, the Voigt profile is well approximated by a Gaussian: $\mathcal{V} = (\sqrt{\pi}b)^{-1} \exp[-(u - y - v_{\parallel}^{\text{IGM}}(y))^2/b^2]$. As stressed by BD97 peculiar velocities affect the optical depth in two different ways: the lines are shifted to a slightly different location and their profiles are altered by velocity gradients. In our modelling, we treat Γ_{-12} as a free parameter, which is varied the observed effective opacity $\tau_{\text{eff}}(z) = -\ln\langle\exp(-\tau)\rangle$ is matched (e.g. McDonald *et al.* 1999; Efsthathiou *et al.* 2000) at the median redshift of the considered range ($\tau_{\text{eff}} = 0.12$ and $\tau_{\text{eff}} = 0.27$ at $z = 2.15$ and $z = 3$, respectively, in our case). We determine Γ_{-12} by requiring that the ensemble averaged effective optical depth is equal to the observed effective optical depth. The transmitted flux is then simply $\mathcal{F} = \exp(-\tau)$.

3.2 Improving the mapping from the linear dark matter density to the non-linear gas density

In this subsection we describe how the mapping from the linear DM density to the non-linear gas density can be improved. As described in the previous section the semi-analytical modelling of Ly α forest spectra involves two main steps:

- smoothing of the linear DM density field to obtain a linear gas density field
- a local mapping from the linear to the non-linear gas density.

In this section we will substitute the log-normal mapping used by BD97 for the second step by a rank-ordered mapping from the linear gas density field to the PDF of the gas density in the hydro-simulation. Figure 1 compares the PDF of the DM density field obtained using SPH interpolation and that of the gas density field. Pressure forces push the gas out into the surrounding voids (‘Jeans smoothing’) and for this reason the PDF of the gas drops below that of the DM density at low densities. At high density the gas is converted into stars and the PDF of the gas density drops again below the PDF of the DM density. As a result the PDF of the gas density is more peaked (Theuns, Schaye & Haehnelt 2000). Figure 2 compares the resulting probability distribution of the flux for simulated spectra using the lognormal model our ‘improved’ model (hereafter PDF model) and the numerical simulations. For this comparison we have produced simulated spectra for the lognormal model and the PDF model with the same cosmological parameters as in our hydrodynamical simulation. We further imposed a power law temperature-density relation with $T_0 = 10^{4.3} \text{ K}$ and $\gamma = 1.2$, which fits the simulation well (Figure 3). The simulated spectra have larger length ($\sim 16000 \text{ km s}^{-1}$) than the spectra extracted from hydro-simulations ($\sim 1400 \text{ km s}^{-1}$),

but are obtained with the same spectral resolution, approximately of 2 km s^{-1} . We take into account that the hydro-simulations is missing large scale power by applying a similar cut-off in the power spectrum used to calculate the semi-analytical spectra. This should allow a fair comparison. The peculiar velocity field is again assumed to be given by linear theory (Eq. 4). All spectra are scaled to $\tau_{\text{eff}} = 0.27$ at $z = 3$ and no noise is added.

The probability distribution of the flux for our PDF model agrees significantly better with that of the spectra obtained from our hydro-dynamical simulation. There are still small but significant differences. While the agreement for this 1 point statistic seems reasonable the agreement becomes very poor for some 2-point statistics of the flux. The function $P(F_1, F_2, \Delta v) dF_1 dF_2$ is the probability that two pixels separated in the spectrum by a velocity difference Δv , have transmitted fluxes in intervals dF_1, dF_2 around F_1 and F_2 , respectively. In the right panel of Figure 2 we show the mean flux difference,

$$\Delta F(F_1, \delta v) = \int P(F_1, F_2, \delta v)(F_1 - F_2) dF_2, \quad (8)$$

for 2 values of F_1 , as a function of Δv (see Miralda-Escudé *et al.* 1997, Theuns *et al.* 2000, Kim *et al.* 2001). The results for the lognormal model and for the PDF model are almost identical, which is not surprising since we checked that the two functions that map the linear density field into the non-linear density field are similar.

For strong absorbers ($0 \leq F \leq 0.1$) the agreement between the numerical simulation and our models which rely on an analytical description of the DM density field is very poor. *What could be the reason for this discrepancy?* We have made the following major simplifications: (i) the peculiar velocity field is assumed to be linear; (ii) we do not simulate the intrinsic scatter present in the relation T_{IGM} vs. δ_{IGM} ; (iii) we recover directly the neutral hydrogen density along the LOS by assuming eq. (6), which is valid only under some assumptions (see Subsection 3.1); (iv) we input only the 1-point probability distribution function of the IGM, without taking into account the higher order moments of the distribution; (v) the correlations are assumed to be those predicted by linear theory, modified by the non-linear mapping, while the correlations of the hydro-simulation are different.

Concerning point (i) it has been shown by Hui *et al.* (1997) that the peculiar velocity field can affect the shape of the absorption features, while it has very small effect on the column density distribution functions of the lines. We have run the calculated spectra varying the peculiar velocity field and have not found a strong dependence of the PDF of the flux on the peculiar velocity quantity. This means that this statistics is mainly influenced by the underlying density field. We have compared the PDF of the peculiar velocity field predicted by linear theory with the peculiar velocity found in the $z = 3$ output of hydro-simulation for the IGM and we have found that the differences are not big. The assumption of a linear velocity field should therefore be a good approximation.

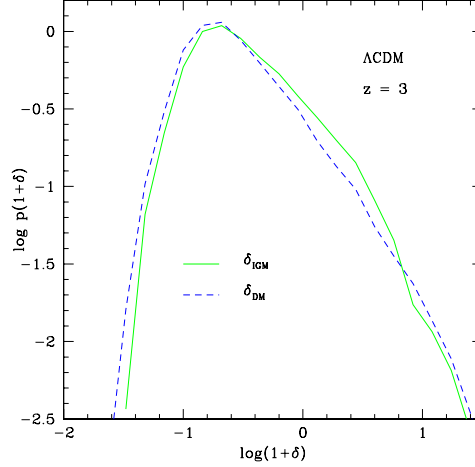


Figure 1. Density distribution of the gas (IGM, continuous line) and dark matter (DM, dashed line) obtained with SPH interpolation over 300 LOS extracted from hydro-simulations at $z = 3$ for an Λ CDM cosmology.

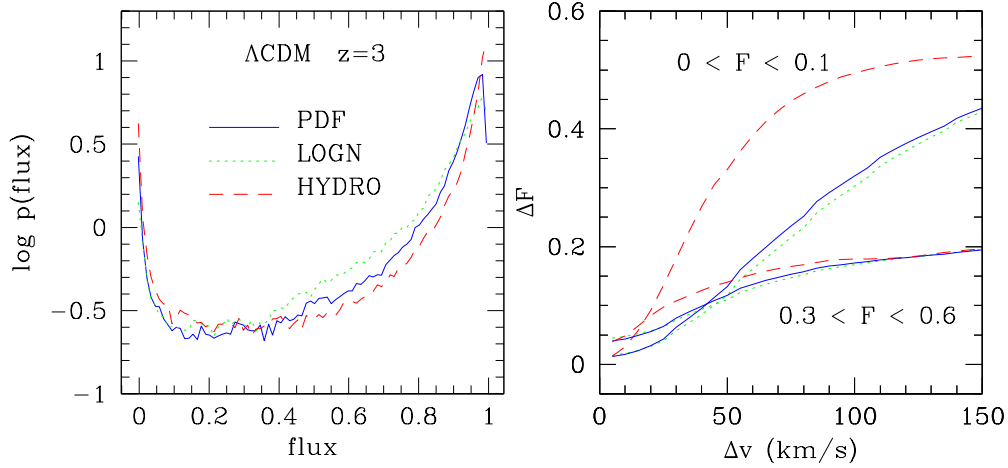


Figure 2. Left panel: one-point function of the flux obtained from the hydro-simulations (dashed line), lognormal model (dotted line) and ‘improved’ model (PDF, continuous line). A total number of $\sim 10^6$ pixels is used in the computation. All the spectra are computed at $z = 3$ for a Λ CDM model. Right panel: mean flux difference $\Delta F(F_1, \delta v)$, for hydro-simulations (dashed line), lognormal model (dotted line) and ‘improved’ model (PDF, continuous line). Two different flux intervals have been chosen which correspond to strong absorbers ($0 < F_1 < 0.1$) and to an intermediate strength lines ($0.3 < F_2 < 0.6$).

If we try to simulate the intrinsic scatter in the relation $T - \delta$, left panel of Figure 3, for example by using as input a higher order polynomial fit instead of the power-law relation, the improvement in the PDF of the flux is negligible. Provided we set the same T_0 of the simulations and a ‘reasonable’ value of γ , the power-law equation of state is a good approximation and the scatter can be neglected.

The same considerations are valid for point (iii). In fact, we have found that eq. (6) is in good agreement with hydro-simulations (Figure 3, right panel), showing that the approximations we made (optical thin limit, high ionisation state) are not affecting the results significantly.

We thus believe that point (iv) and (v) are the main simplification involved in the model. This is somewhat expected as in the definition of the optical depth, eq. (7),

the summation is done over nearby pixels, so it is influenced by the spatial correlations, which are assumed to be those predicted by the linear theory, modified by the local non-linear mapping. In the following Sections we will thus turn to models that are based on the DM density field obtained directly from a N -body simulation (Fig. 14 below). These models reproduce the flux correlation for strong absorbers much better. This demonstrates that correlations in the density field introduced by the non-linear evolution are indeed responsible for the shape of strong lines. These are not reproduced accurately by our local mapping from the linear to non-linear gas density. The marked differences for strong absorbers are not unexpected as the $z = 3$ output of hydro-simulation contains very strong absorption systems from fully collapsed objects which are not related to the Ly α forest. The spectra of the LOGN model have been pro-

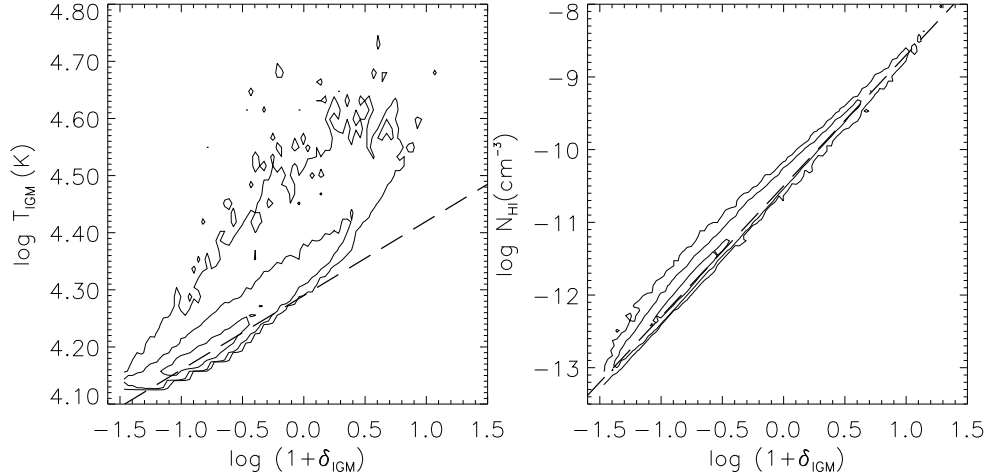


Figure 3. Left panel: contour plot of $\log(T_{IGM})$ vs. $\log(1 + \delta_{IGM})$, at $z = 3$. The dashed line is obtained by setting $\gamma = 1.2$. Right panel: contour plot of $\log(N_{HI})$ (comoving neutral hydrogen density in cm^{-3}) vs. $\log(1 + \delta_{IGM})$ obtained from the $z = 3$ output of the hydro-simulation. The dashed line is given by eq. (6). Levels of contours increase by a factor 10. (a total number of 3×10^5 points is used in the computation).

duced using the Jeans length at the mean temperature and with a fixed value of γ . If we use other values for the temperature T_0 and for γ we can obtain a better agreement in other flux intervals. In Figure 2 the range of flux values in which the agreement with the flux PDF of the hydro-dynamical simulation and in ΔF is good corresponds to intermediate absorbers ($0.2 < F < 0.4$), this is in part determined by the requirement of having a fixed $\tau_{eff} = 0.27$ for the ensemble of simulated spectra in each model, which scales the neutral hydrogen fraction.

4 MODELS USING NUMERICAL SIMULATIONS OF THE DARK MATTER DISTRIBUTION

4.1 Zel'dovich modelling of the gas distribution

In this Section we present models of the gas distribution based on a modified filtering of the initial conditions of the dark matter density field. The first method is based on the truncated Zel'dovich approximation (TZA). Among the possible approximations, TZA has been found to produce the best agreement with N-body results (see Coles *et al.* 1993, Melott *et al.* 1994, Sathyaprakash *et al.* 1995). Hui *et al.* (1997, hereafter HGZ) showed that the TZA, with an appropriate smoothing and with a recipe which allows to convert density peaks into absorption lines, successfully reproduces the observed column density distribution of the Ly α forest lines over a wide range of N_{HI} . Gnedin & Hui (1998) presented a more accurate semi-analytical model of the Ly α forest by combining a particle mesh solver modified to compute also an effective potential due to gas pressure. They showed that a particle mesh solver, with an appropriate filtering of the initial condition, can be used to model the low density IGM. All these differ-

ent methods have the advantage of being much faster than a hydro-simulation. Given these results we are now going to use the same tools to make a comparison, LOS by LOS, between the simulated gas distribution and the effective gas distribution of the $z = 3$ output of the hydro-simulation. Our simulation is significantly larger and with higher resolution than that used by Gnedin & Hui (1998).

Following Hui *et al.* (1997), we define a non-linear wavenumber k_{nl} (see also Melott *et al.* 1994):

$$D_+^2(z) \int_0^{k_{nl}} P(k) d^3\mathbf{k} = 1, \quad (9)$$

where $D_+(z)$ is the linear growth factor for the density perturbations and $P(k)$ the linear power-spectrum. We filter the linear density field with a Gaussian window $W(k, k_s) = \exp(-k^2/2k_s^2)$, with $k_s \sim 1.5k_{nl}$. At this point we displace particles from the initial Lagrangian coordinates \mathbf{q} according to the truncated Zel'dovich approximation:

$$\mathbf{x}(\mathbf{q}, z) = \mathbf{q} + D_+(z) \nabla_{\mathbf{q}} \phi_f(\mathbf{q}), \quad (10)$$

with $\phi_f(q)$ the initial *filtered* velocity potential (see *e.g.* Coles *et al.* 1995), with $\phi(\mathbf{k})$ the actual potential used in the initial conditions of the simulation. The filtering is intended to prevent shell-crossing. To mimic baryonic pressure, we smooth the initial density field with a Gaussian window $\exp(-k^2/2k_J^2)$, with k_J given by eq. (2), as in HGZ. The final filtering scale is effectively the smaller of k_s and k_J . In our case, $k_s \sim 5.5 \text{Mpc}^{-1}$ and $k_J \sim 7 \text{Mpc}^{-1}$, these wave numbers correspond to scales of $\lambda_s \sim 1.14 \text{Mpc}$ and $\lambda_J \sim 0.9 \text{Mpc}$, respectively. This means that the amount of filtering, before displacing particles, is given by the condition of eq. (9).

We also outline here a further approach based on the assumption that the displacement between DM and IGM particles is ‘Zel’dovich-like’. We refer to this

method as the Zel'dovich Displacement (ZD method). The difference, at redshift z , between the Eulerian position of a gas and a DM particle which have the same Lagrangian coordinate \mathbf{q} , according to the Zel'dovich approximation, is:

$$\Delta\mathbf{x}(\mathbf{q}, z) = D_+(z)[\nabla_{\mathbf{q}}\psi_{IGM}(\mathbf{q}, z) - \nabla_{\mathbf{q}}\phi_{DM}(\mathbf{q})], \quad (11)$$

where ψ_{IGM} and ϕ_{DM} are the IGM and DM velocity potentials. In Fourier space we have (Matarrese & Mohayaee 2002) $\psi_{IGM}(\mathbf{k}, z) = W_{IGM}(\mathbf{k}, z)\phi_{DM}(\mathbf{k})$ and from eq. (11) we get:

$$\Delta\mathbf{x}(\mathbf{k}, z) = D_+(z)[W_{IGM} - 1]i\mathbf{k}\phi_{DM}(\mathbf{k}). \quad (12)$$

The above equation shows that for $k \ll k_J$ $W_{IGM} \rightarrow 1$, $\Delta\mathbf{x}(\mathbf{k}, z) \rightarrow 0$, while for $k \gg k_J$, $W_{IGM} \rightarrow 0$, $\Delta\mathbf{x}(\mathbf{k}, z) \rightarrow -i\mathbf{k}\phi_{DM}(\mathbf{k})$. In the first limit, Jeans smoothing is not effective and the IGM traces the DM, in the second limit the effect of gas pressure prevents large displacements of baryons from their initial location. According to this method, the displacement between DM and IGM particles with the same Lagrangian coordinate is given by a filtering of the initial DM density field. We calculate this displacement at $z = 3$ with the filter proposed by Gnedin & Hui (1998), *i.e.* instead of W_{IGM} we use $W_{ZD} = \exp(-k^2/2k_{ZD}^2)$, with $k_{ZD} \sim 2.2k_J$. This choice is motivated by the fact that a Gaussian filter gives an excellent fit to baryon fluctuations for a wide range of wave numbers. The filtering scale k_{ZD} is the value predicted by linear theory at $z = 3$, assuming that reionization takes places at $z \sim 7$ (Gnedin & Hui 1998). The location of the gas particle is then found by adding this displacement to the *actual position* at $z = 3$ of the DM particle with the same Lagrangian coordinate.

In Figure 4 we show four panels, which are slices of thickness $\sim 0.1 h^{-1}$ comoving Mpc at the same position along the z -axis, for the IGM and the DM distribution of the hydro-simulations (top panels), the TZA field (bottom left panel) and the IGM field obtained with ZD method (bottom right).

By comparing the top panels, one can see that the gas is more diffuse than the dark matter. TZA reproduces the main filaments but we know that the agreement will be better in the low-density regions. ZD (with a filtering at $k_{ZD} \sim 16\text{Mpc}^{-1}$) seems promising, at least by eye. This method allows some diffusion around the dark matter to reproduce the gas distribution. A more quantitative comparison is needed to see how good our IGM density field is compared to the hydro one. We compare LOS by LOS the SPH interpolated IGM density fields with the ‘true’ IGM field of the hydro-simulation. This test is pretty severe as we are not going to filter the density fields and the comparison is made ‘pixel-by-pixel’.

The results are shown in Figure 5 where we compare the amount of scatter predicted by the TZA approximation (left panel) and the ZD method (right panel). As expected, the test without any filtering on the *final* density field shows that the TZA tracks the simulation, but the scatter is very large. The ZD method agrees better with the simulation, but the scatter is still rather significant. A more detailed comparison is shown in Figure 6,

where we plot the mean, and scatter around the mean, as a function of density.

Clearly ZD works significantly better than TZA, the average value is better reproduced and also the scatter is significantly smaller. The amount of scatter and the average value found with the ZD method are consistent with the results of Gnedin & Hui (1998; see their Figure 4).

4.2 Using the mean $\delta_{DM} - \delta_{IGM}$ relation of the hydro simulation to predict the gas distribution from the DM distribution.

The results of the previous section have demonstrated that ‘filtering’ techniques on the initial conditions do not result in density fields that agree well with hydro-simulations, at least for a ‘pixel-by-pixel’ comparison with a high-resolution simulation.

In this section we present an alternative approach that starts from the actual DM density distribution of the numerical simulation and ‘predicts’ the gas distribution using a fit to the mean relation between gas and DM density. In this way the displacement of the gas with respect to the dark matter is modelled statistically in *real space*. The techniques of the previous Section are all based on different filtering schemes which smooth the IGM density field over a constant scale set by the Jeans length *at the mean density*. This filtering is done in *Fourier space* and leads to equal smoothing of all dark matter structures independent of their density. As discussed above this strong simplification is responsible for the rather strong discrepancies with the gas distribution in our hydro-dynamical simulation.

In Figure 7 we plot IGM and DM over densities, IGM peculiar velocity and IGM temperature obtained with SPH interpolation (see Appendix A for details). The figure demonstrates that a simple relation between the DM and the gas IGM density fields does not exist. For a wide range of moderate over densities, *i.e.* $-0.75 \lesssim \delta \lesssim 5$, the PDF of the gas distribution lies above that of the DM (Fig. 1): this of course does not determine the relation between gas and dark matter, but shows that we should expect a significant number of regions in which δ_{IGM} is larger than δ_{DM} .

This is what we see in panels (a) and (b) of Figure 7. There are regions at $\delta \lesssim 10$ where the gas is more concentrated than the dark matter *e.g.* at $v \sim 170 \text{ km s}^{-1}$ in panel (c). At low δ there is an almost perfect agreement between the gas and the dark matter distribution, while at moderate and large over densities the relation between gas and dark matter is not unique. To investigate further we also show the temperature and peculiar velocity along these LOS. The highest density peak in panel (d) is related to a peak in the temperature of the gas of $10^{4.9} \text{ K}$ and a strong gradient in its peculiar velocity, suggesting the presence of a shock. However, if we look at panel (a), the peak in the gas density at $v \sim 50 \text{ km s}^{-1}$ is more peaked than the DM, while the velocity field and the temperature show no particular behaviour. This means that modelling of the gas distribution using only the information along the LOS will not be very accurate on a point-to-point basis, but we

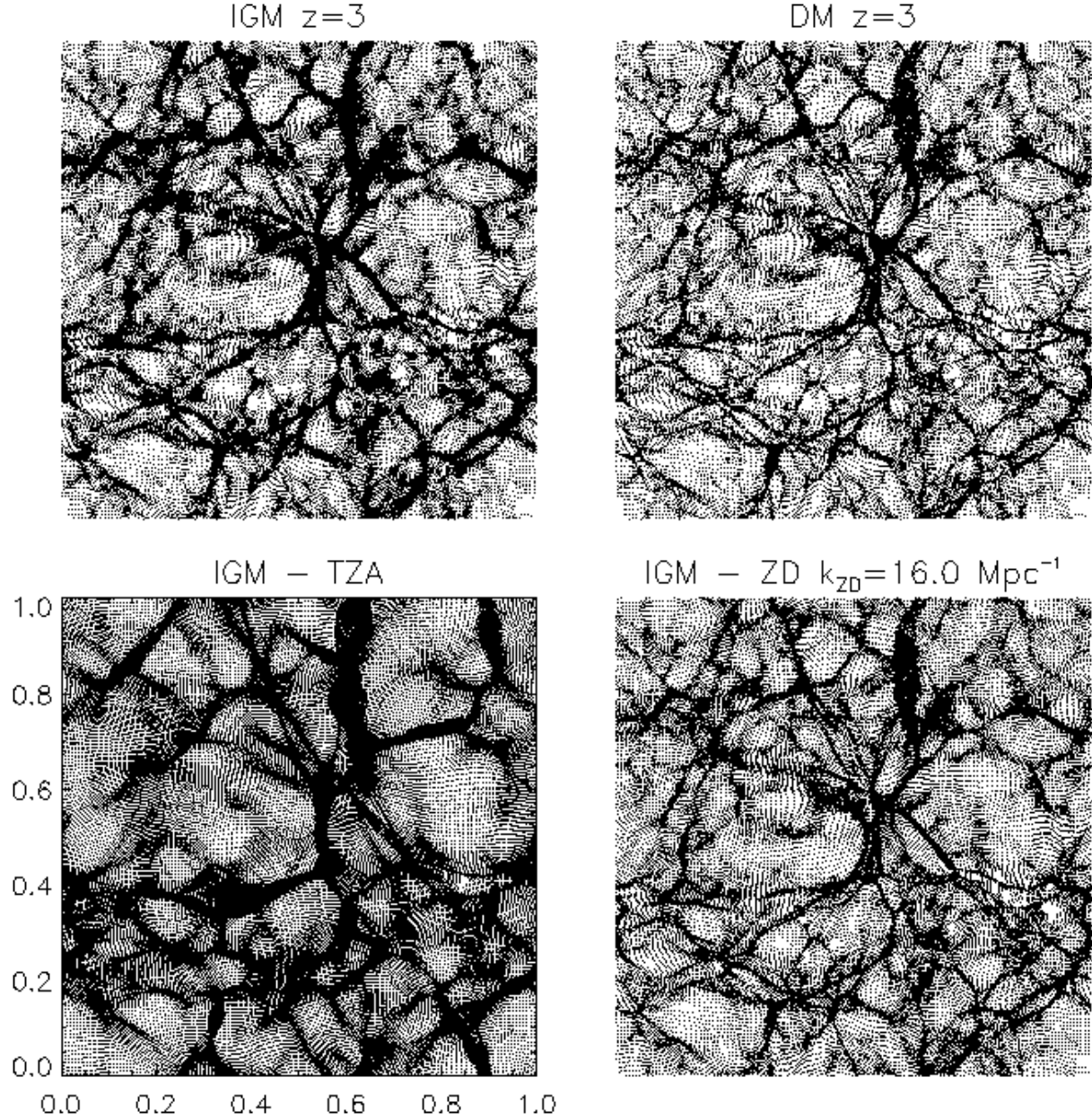


Figure 4. Slices along the z -axis of thickness $\sim 0.1h^{-1}$ comoving Mpc (coordinates in normalised units). Top panels: IGM distribution (left) and DM distribution (right), from the $z = 3$ output of the Λ CDM model. Bottom panels: Zel'dovich modelling of the IGM distribution from the initial conditions of hydro-simulation (left panel, TZA), Zel'dovich displacement added to DM particles to mimic baryonic pressure (right panel, ZD).

might nevertheless hope to obtain a model for the gas distribution which has the correct properties in a statistical sense.

We start by plotting the values of δ_{IGM} vs. δ_{DM} obtained from the simulation at different redshifts. Figure 8 demonstrates that the scatter between the IGM and DM densities increases with decreasing redshift, as expected. At $z = 10$, there is almost perfect agreement between the two fields, but when cosmic structures get non-linear the physics becomes more complex. In addition, reionization occurs in our simulation at $z \sim 6$, so before that the simulations do not resolve the then much

smaller Jeans length. At later redshifts, the effect of the baryonic pressure can be seen. For under dense regions, the IGM density tends to be higher than the DM density, because pressure is pushing gas into the low density voids. For larger values of δ_{DM} the scatter increases and gas can be either denser or less concentrated than the dark matter, depending on star formation which sets-in in the simulations at over densities ≥ 80 (see Aguirre, Schaye and Theuns 2002 for a more detailed description of the star formation recipe adopted).

We fit the relation between gas and DM density with a 3rd order polynomial; the results are shown in

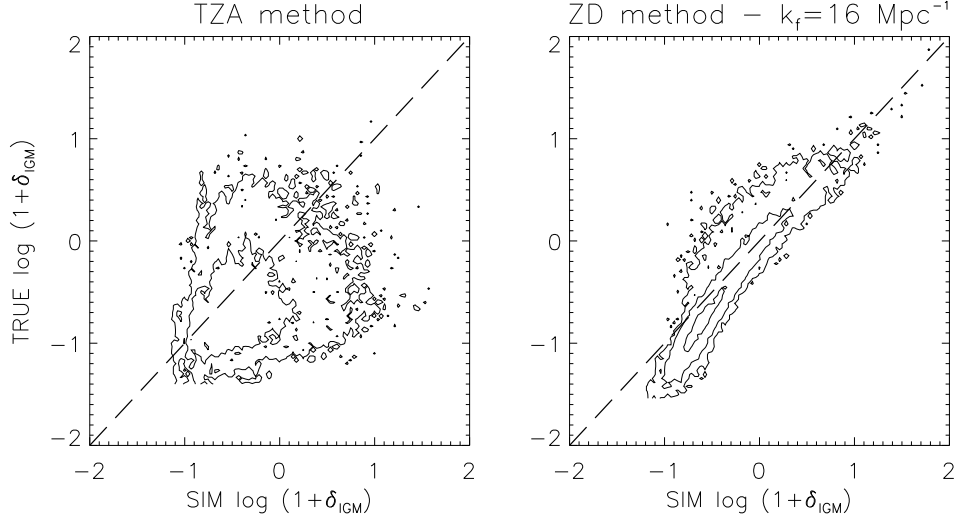


Figure 5. Contour plots of the true IGM over density derived from the hydro-simulation and the simulated IGM over densities obtained with the truncated Zel’dovich approximation (TZA, left panel) and the ‘Zel’dovich displaced’ method (ZD, right panel), at $z = 3$. k_f for ZD is $\sim 16 \text{ Mpc}^{-1}$, k_s for TZA is $\sim 5.5 \text{ Mpc}^{-1}$. In both the panels, the number density of the elements increases by an order of magnitude with each contour level (a total number of 3×10^5 points are used in the computation).

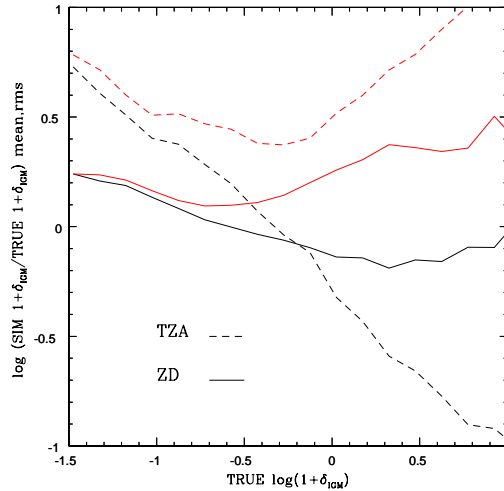


Figure 6. Average and rms value of the difference between $\log \text{SIM}(1+\delta_{IGM})$ and $\log \text{TRUE}(1+\delta_{IGM})$, with the TZA (dashed) and ZD method (continuous). Thick lines represent the rms values, thin lines the average.

Figure 9, where the range of δ_{DM} plotted is the one of interest for the Ly α forest, $-1 \lesssim \delta \lesssim 6$. If we set $y = \log(1+\delta_{IGM})$ and $x = \log(1+\delta_{DM})$ the fitting function is:

$$y = 0.02^{\pm 0.03} + 0.91^{\pm 0.05} x - 0.15^{\pm 0.05} x^2 - 0.08^{\pm 0.04} x^3, \quad -1.5 \leq x \leq 1.0, \quad (13)$$

where the errors reported are the 1σ uncertainties of each coefficient. The same function has been found to be a reasonable good fit at $z = 4$ and $z = 2$ as well, so it can be used to simulate the gas distribution in this redshift range for a Λ CDM model. From Figure 9 one can see that the fitting function predicts that the gas is on average more concentrated than the dark matter for a wide range of δ_{DM} , although significant scatter is present.

Is it possible to reduce this scatter using other information?

In Figure 10 (left panel) we plot the peculiar velocity gradient of the dark matter density fields vs. the difference Δ between the ‘true’ value of $\log(1+\delta_{IGM})$ and the ‘fit’ value obtained with eq. (13). Both these quantities have been smoothed over a scale of $\sim 100 \text{ km s}^{-1}$ to reduce noise. Δ is weakly anti-correlated with the dark matter peculiar velocity gradient, with regions with a negative gradient lying above the mean fit and hence have $\Delta > 0$. On average, a negative velocity gradient indicates that the gas is being compressed and so may be undergoing moderate or strong shocks. As a consequence, the gas is also being heated, and this introduces the correlation between Δ and the temperature of the gas (Fig. 10, right panel). This correlation is stronger, because the gas temperature is a more direct indicator

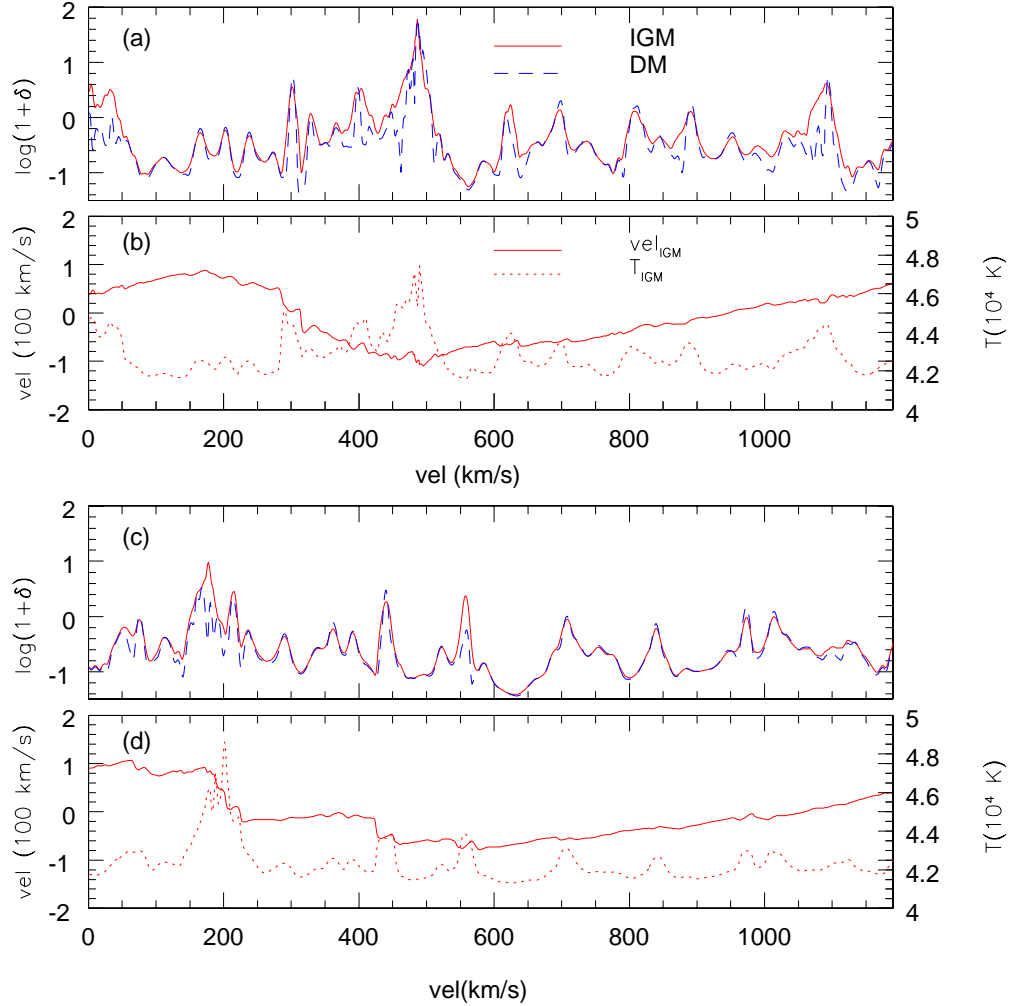


Figure 7. Two different LOS at $z = 3$ from the hydro-simulation. Panel (a): density contrast for the IGM (continuous line) and DM (dashed line), obtained with SPH interpolation. Panel (b): the peculiar velocity field, in units of 100 km s^{-1} for the IGM (continuous line) and temperature of the IGM, in units of 10^4 K (dotted line). Panels (c) and (d): the same quantities are shown but for a different LOS.

of a shock. Conversely, negative Δ , *i.e.* points below the fitting function, are related to colder regions of gas and small positive gradients of the dark matter peculiar velocity field. As expected, the bulk of the points is in quiet regions with $dv_{pec}/dx \sim 0$ and temperatures between $10^{4.2} \text{ K}$ and $10^{4.3} \text{ K}$.

These results suggest that we can indeed model the gas distribution that corresponds to a given dark matter density and peculiar velocity distribution statistically. We use the fit of eq. (13) to predict the gas density field from the dark matter density field. The modelling can be further improved by taking the peculiar velocity of the dark matter into account. For this purpose we fit the relation shown in the left panel of Figure 10 with a 2nd order polynomial because the correlation is weak. Models obtained using the density-density fit and models using a two parameter density-density plus the density-peculiar velocity fit will be referred to as FIT-1 or FIT-2, respectively.

The fitting function of eq. (13) gives a good approximation to the gas distribution for a ΛCDM model in the

redshift range $2 \lesssim z \lesssim 4$. The same technique can be applied to other cosmological models and different redshift ranges. We will now make a LOS by LOS comparison for the the gas density distribution of the two models FIT-1 and FIT-2 to that of our hydro-dynamical simulation. In Figure 12 we show the scatter plots for the gas (over)densities for the two models. Figure 11 shows the scatter in terms of the standard and mean deviation for both models. The simple DM model where the gas is assumed to trace the dark matter exactly is also shown (thick, thin and dotted lines, respectively).

Figure 12 illustrates the improvement of using the fitting procedure of model FIT-2. The χ^2 for these fits, where $\chi^2 \equiv N_{bin}^{-1} \sum_{i=1}^{N_{bin}} \frac{(\delta_i - \bar{\delta})^2}{\sigma_i^2}$ ($N_{bin} = 25$ is the number of bins) are 0.24, 0.21 and 0.19 for the FIT-1, FIT-2 and DM, respectively, showing that the scatter is effectively reduced with the second method but still in the total interval $-1.5 < \log(1 + \delta_{IGM}) < 1$.

When the density range is constrained to be in the interval $-1 < \log(1 + \delta_{IGM}) < 0.6$, relevant for the Lyman α forest, we obtain χ^2 of 0.06, 0.03 and 0.10 for

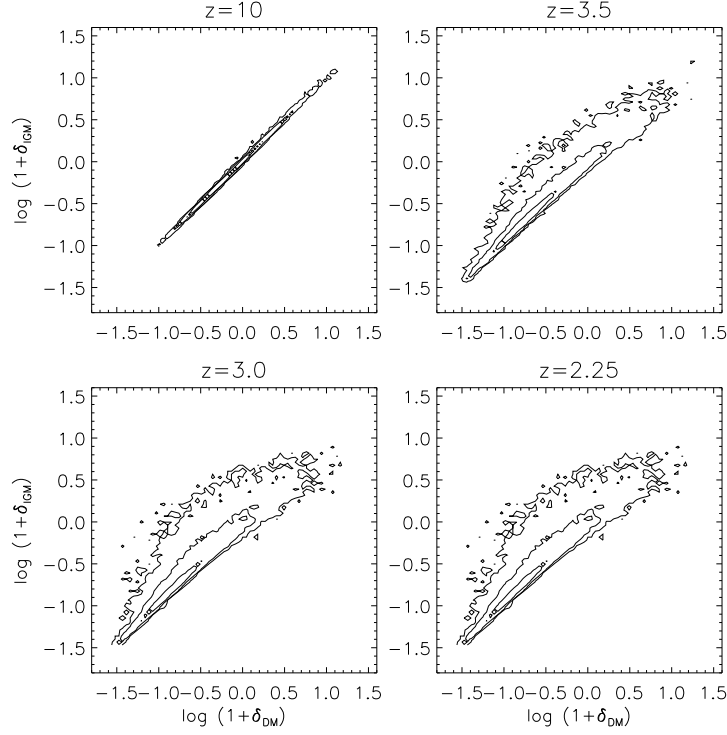


Figure 8. Scatter plots of $\log(1 + \delta_{IGM})$ vs. $\log(1 + \delta_{DM})$, at $z = 10$ (top left), $z = 4$ (top right), $z = 3$ (bottom left) and $z = 2.25$ (bottom right) of the hydro-simulation. 30 LOS of 2^{10} pixels are reported here.

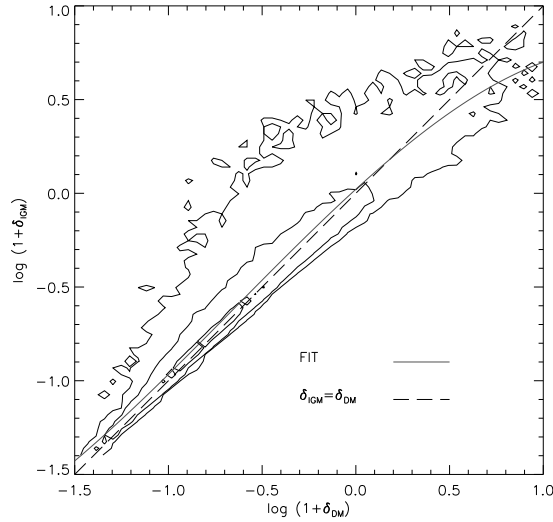


Figure 9. IGM density contrast vs. DM density contrast, at $z = 3$ for the Λ CDM model. The continuous line is the 3rd order polynomial fit, the dashed line is obtained by setting $\delta_{IGM} = \delta_{DM}$.

the FIT-1, FIT-2 and DM model respectively, illustrating the improvement of the fitting procedure. Comparing with Figure 6, we see that the FIT-2 method is significantly better than ZD in reproducing the mean values for $\log(1 + \delta_{IGM}) \lesssim 0.5$ (however, for larger over densities ZD shows a better agreement than FIT-2 or

FIT-1), while the rms values are basically equivalent. If we apply the fitting procedure in the range $\delta_{IGM} \lesssim 1$ which represents the bulk of the IGM, the mean and rms deviation between the fitted and true IGM densities are smaller than 10 and 30 per cent, respectively.

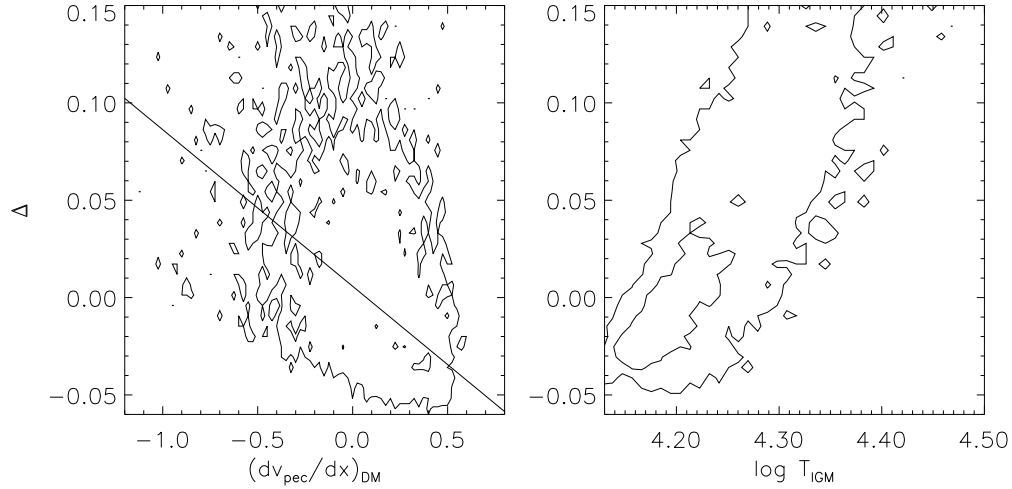


Figure 10. Scatter plots of the dark matter peculiar velocity gradient along the LOS vs. Δ (left panel) and temperature of the IGM vs. Δ (right panel), where $\Delta = \log(1 + \delta_{IGM}) - \text{fit}$, i.e. the difference between the true value and the value obtained with the fit, (see eq. 13). Weak correlations are present.

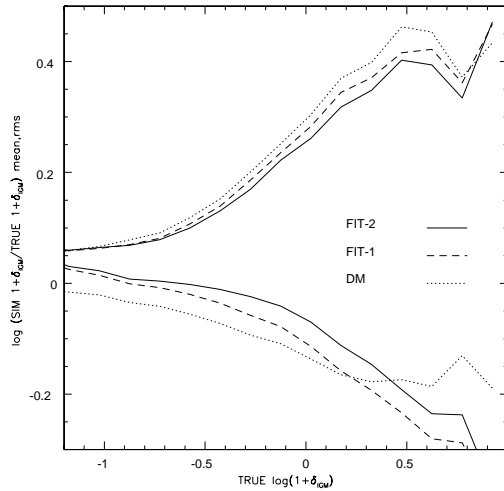


Figure 11. Average (thin lines) and rms (thick lines) value of the difference between $\log \text{SIM}(1 + \delta_{IGM})$ and $\log \text{TRUE}(1 + \delta_{IGM})$, for the FIT-2 (continuous lines), FIT-1 (dashed lines) and DM (dotted lines) methods.

4.3 Jeans smoothing of the evolved DM density field

Here we investigate the effect of smoothing the evolved rather than the initial DM density field on a constant scale set by the Jeans length at mean density. We use the DM distribution of the $z = 3$ output of the hydro-simulation to compute the dark matter density field on a cube of 128^3 mesh points using SPH interpolation as described in the Appendix. The cell size of this mesh of ≈ 0.14 co-moving Mpc approximately resolves the Jeans length $\lambda_J \sim 1$ Mpc. We have to choose a mesh because the filtering is done in 3D using fast Fourier transforms. However, we note that also 1D smoothing along LOS is in rough agreement with the 3D one. To model the Jeans smoothing we convolve the DM density field with a Gaussian filter $W = \exp(-k^2/2k_f^2)$, with $k_f = k_J \sim 7 \text{Mpc}^{-1}$. By comparing Figure 9 with Fig-

ure 13 one can see that the Jeans smoothed dark matter density field is very different from IGM distribution in the hydro-simulation. Given this large discrepancy between hydro-simulations and Jeans smoothed dark-matter density field we choose not to analyse into the details the density statistics as we did for the models of the previous subsection.

The main reason for the large difference between the true IGM density distribution, and the one obtained from Jeans smoothing the DM density field, is the simplification of a constant smoothing length. In reality, the Jeans length depends on temperature, and therefore should be adaptive. Unfortunately, Fourier space filtering techniques smooth all structures in the same way, since they are global operations. In low-density regions, the amount of smoothing in hydrodynamical simulations is small, but the Jeans smoothed density

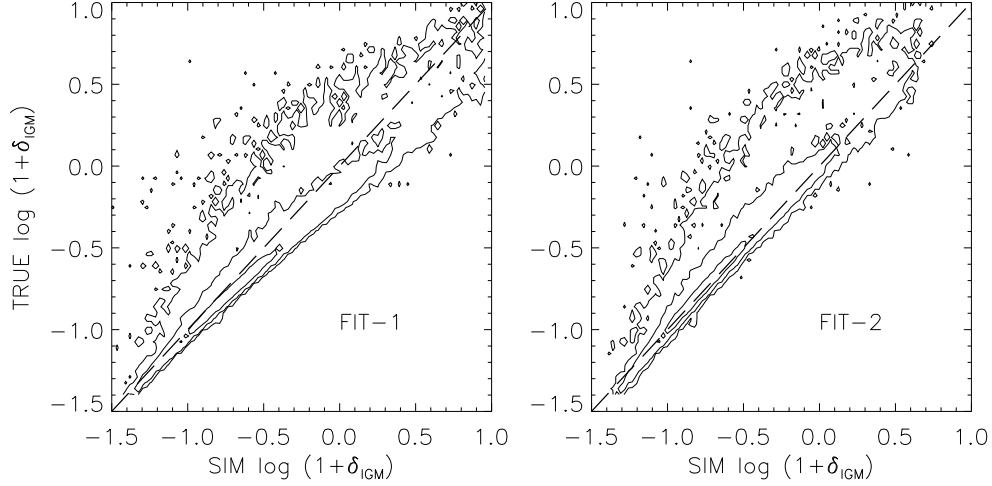


Figure 12. Left panel: true versus simulated (FIT-1 model, Eq. 13) δ_{IGM} at $z = 3$ for the Λ CDM simulation plotted vs simulated δ_{IGM} (FIT-1 model) obtained with the fit of eq. (13). Right panel: true δ_{IGM} versus that obtained using FIT-2 model, improved with the fitting of the scatter (see Figure 10). Contour levels are off-set by 1 dex, and are based on 3×10^5 points.

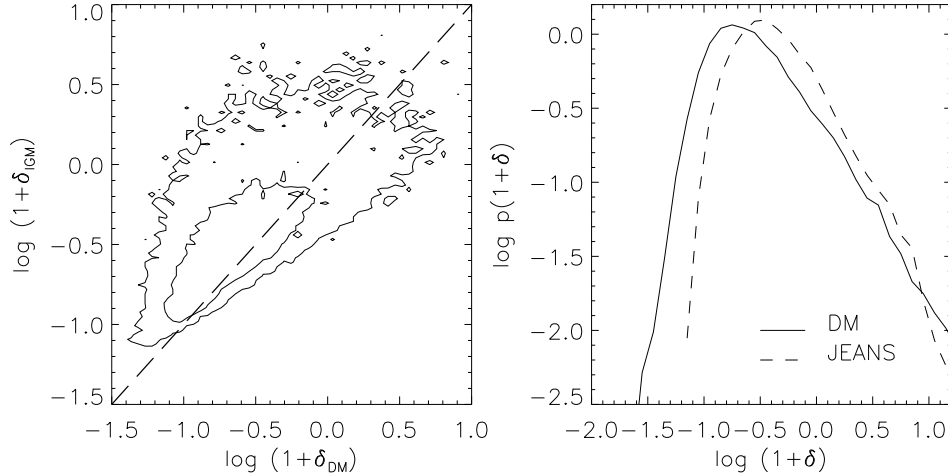


Figure 13. Left panel: scatter plot of the dark matter density field smoothed on the Jeans length at $z = 3$ and the dark matter density field; both these fields are evaluated with SPH interpolation in 128^3 mesh points. 3×10^5 points are shown; the 1 line is obtained by setting $\delta_{IGM} = \delta_{DM}$. This plot has to be compared with Figure 9, which shows the results from hydro-simulations. Right panel: PDF of the dark matter (continuous line) and PDF of the Jeans smoothed dark matter density field (dashed line).

field is very different from the original DM field. On the other hand, for large over densities of the dark matter, Jeans filtering at the mean gas density underestimates the amount of smoothing, the region at $\delta_{IGM} < \delta_{DM}$, for large values of δ_{DM} , is more populated in Figure 13 than in Figure 9. As we will see in the next section the resulting flux statistics are very different as well.

5 A COMPARISON OF FLUX STATISTICS FOR THE IMPROVED METHODS

In this section we compare the flux distribution obtained with the different methods for modelling the gas density field. Figure 14 shows the 1-point probability dis-

tribution function for the flux (left panel) and the mean flux difference ΔF (Eq. 8, right panel), for three models: (i) DM (dotted line) is the PDF we get by setting $\delta_{IGM} = \delta_{DM}$; (ii) ZD (dashed lines) is the PDF obtained with the ‘Zel’dovich Displacement’ method of Section 4.1 with a $k_f \sim 16 \text{ Mpc}^{-1}$; (iii) FIT-2 (continuous line) is the PDF obtained with the fitting technique of the previous Section and adding the scatter inferred from the dark matter peculiar velocity field. We also show the flux PDF of the hydro-dynamical simulation (triangles) which is the true PDF extracted from the $z = 3$ output of the Λ CDM model.

All these methods try to predict the gas distribution from the dark matter distribution of the numerical

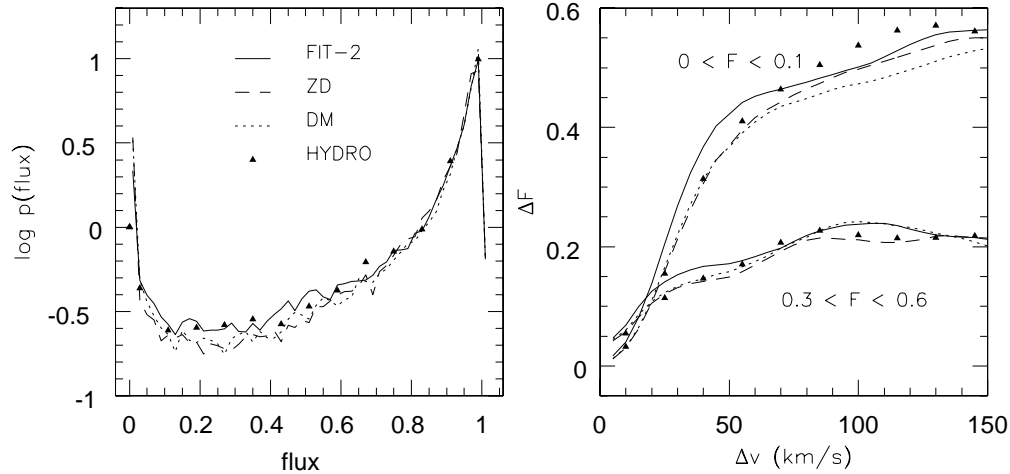


Figure 14. PDF of the flux (left panel) and ΔF which, is related to the 2-point PDF of the flux (right panel). Comparison between different methods: FIT-2 (continuous line), ZD (dashed), DM (dotted). The PDFs extracted from hydro simulations are represented by the triangles (HYDRO). This plot has to be compared with Figure (2).

simulation. We thereby assume that $v_{HI} \sim v_{IGM} \sim v_{DM}$ which we have checked to be a good approximation. The local abundance of neutral hydrogen is computed from the ionisation equilibrium equation, eq. (6). We further need to assume the temperature at mean density, T_0 , and the slope of the temperature-density relation, γ . We take $T_0 = 10^{4.3} \text{K}$ and $\gamma = 1.2$. All simulated spectra have been scaled to the same effective optical depth, $\tau_{eff} \sim 0.27$ (which is a good fit to the observed effective optical depth at redshift $z = 3$).

The PDF of the flux is very similar for the three models. We performed a quantitative comparison based on the Kolmogorov-Smirnov (KS) test which characterises the difference between two models from the maximum absolute deviation, d_{KS} , between the two cumulative flux distributions (see Meiksin *et al.* 2001 for further details on KS test applied to the PDF of the flux). We calculate d_{KS} for the lognormal model (LOGN) and the ‘improved’ model (PDF) obtained by implementing the 1-point probability distribution function of the IGM as well. Fluxes obtained with TZA have not been computed as the large scatter found (left panel, Figure 5) suggests that this approximation is the least accurate. The KS test was performed for a total of $\sim 10^4$ pixels (Table 5).

The best agreement with the hydro-simulation is obtained with the FIT-2 method. The KS indicates a slightly better agreement than for the FIT-1 method. The ZD method gives better agreement than assuming that the gas traces the dark matter. The PDF and LOGN methods are the least accurate; this means that our fitting methods are indeed a significant improvement.

Model	d_{KS}
FIT-2	0.028
FIT-1	0.032
ZD	0.035
DM	0.039
PDF	0.098
LOGN	0.144

The methods based on the actual DM density distribution (FIT-1, FIT-2, DM) also reproduce the 2-point flux distribution of the hydro-simulation dramatically better than those based on linear theory or the lognormal model as can be seen by comparing Fig. 14 (right panel) with Fig. 2. Note especially the significant improvement in the shape of strong lines. As discussed above this implies that this statistic is mainly influenced by the correlations in the underlying dark matter density fields which are now the same for all the models.

We choose to make a final plot to quantify the differences between the Jeans smoothed dark matter density field and the hydro-simulations in terms of the PDF of the flux. Results are shown in Figure 15. The number of pixels per LOS is 128, significantly lower than in the comparisons between the other improved methods 4.2. To produce ‘Jeans smoothed’ spectra we assume again that $v_{HI} \sim v_{DM}$ and a power-law equation of state for the dark matter over density. This time there are also significant differences between the two models also in terms of the PDF of the flux. The hydro PDF predicts more dense regions than the Jeans smoothed one, and correspondingly less regions with small densities. This is somewhat counterintuitive, since the fitting technique smooths less in low density regions compared with Jeans smoothing. However, we require both types of spectra to have the same τ_{eff} . Effectively, this means that the two PDFs for δ are multiplied by a correction factor, which can be seen as a scaling of the neutral hydrogen, in such a way that the hydro PDF has a larger number

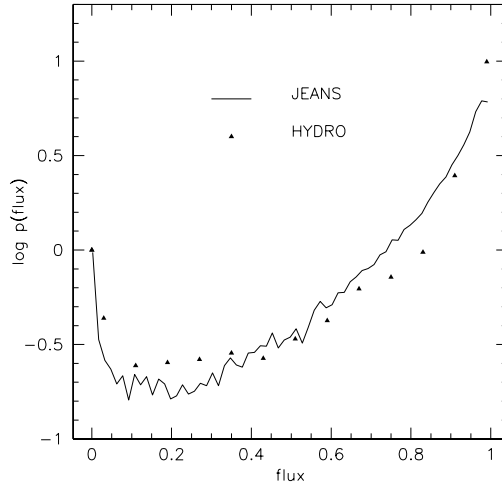


Figure 15. PDF of the flux obtained from the Jeans smoothed dark-matter density field (continuous line). Filled triangles represent the hydro-simulation PDF.

of regions at large δ than the Jeans smoothed field. The d_{KS} of the two distribution is ~ 0.1 slightly better than the LOGN model value.

The main conclusions of this Section are: (i) the use of the numerically simulated dark matter density distribution for the prediction of the gas density distribution results in a significant improvement in the comparison with the hydro-simulations; (ii) the modelling of the gas distribution using the fit to the mean relation between dark matter and gas density in the hydro-simulations results in much better agreement than the methods where a filtering scheme is applied to the initial or evolved density field.

6 DISCUSSION AND CONCLUSIONS

Many aspects of the warm photo-ionised Intergalactic medium can be well modelled by hydrodynamical simulations. These are, however, still rather limited in dynamic range and lack the possibility of extensive parameter studies due to limited computational resources. In order to overcome these problems we have tested several approximate methods for simulating the Ly α forest in QSO absorption spectra. The modelling consists of two main steps (i) modelling the DM distribution and (ii) mapping the DM distribution into a gas distribution.

Methods which use an analytic description of the DM distribution like the lognormal model give a rather poor description of the gas distribution compared to numerical simulations. In Section 3 we have shown that this results in flux PDFs which are in rough agreement with the PDF extracted from hydro-simulations. The agreement can be improved with a variant of the log-normal model where a mapping between linear and non-linear IGM density fields calibrated by hydro-dynamical simulations is used. However, in both cases, the 2-point PDF of the flux differs significantly from that obtained from numerical simulations. This is because the 2-point PDF is strongly affected by the underlying correlations in the DM density field, which are not well reproduced

in models based on an extrapolation of linear theory. To take properly account of these correlations on a point-to-point basis numerical DM simulations are required.

We thus tested a variety of schemes to relate the DM distribution of numerical simulations to the gas distribution. These schemes are supposed to take into account that the gas is smoothed on a Jeans scale relative to the dark matter. We first investigated two approximations based on the Zel'dovich approximation, the truncated Zel'dovich approximation (TZA) and a scheme which we call Zel'dovich displacement (ZD). The latter is based on the assumption that the displacement between DM and IGM at the same Lagrangian coordinate depends on the initial DM density field, filtered on a suitable scale. The TZA reproduces the gas density field very poorly in a LOS by LOS comparison. It is actually worse than if we assume that the gas traces the DM faithfully. The ZD method which allows diffusion on a scale smaller than half of the Jeans length to mimic baryonic pressure fares somewhat better. The scatter in plots of predicted vs. simulated densities is nevertheless only slightly smaller than in a model where gas traces dark matter. We have also tested the ZD method with smoothing on a global Jeans length and have again found poor agreement with spectra extracted from hydro-simulations. It may be that filtering techniques based on the Zel'dovich approximation can reproduce some statistical properties of the Ly α forest like the column density distribution reasonably well, but they fail in reproducing the flux distribution in detail.

To make progress we have thus investigated the relation of the gas density and the DM density in the hydro-dynamical simulation in more detail. The relation between δ_{IGM} and δ_{DM} can be well fit with a 3rd order polynomial. There is considerable scatter around the mean relation and we have examined the correlations between deviations from the fit with other physical quantities along the LOS. There is a weak correlation of these deviations with the filtered dark matter peculiar velocity gradient and a somewhat stronger correlations with the gas temperature. This indicates that the devi-

ations are due to moderate or strong shocks in the gas component.

Combining the DM simulations with the fitted relation between DM density and gas density gives good results for both the one and two-point distribution of the flux. If we introduce an additional correlation of the gas density with the DM peculiar velocity gradient as found in the hydro simulations the agreement is further improved (a method which we called FIT-2). These fitting methods give significantly better results than the other methods we have discussed.

Smoothing of the dark matter density field with a constant global Jeans scale calculated for mean density and temperature results in a gas distribution very different from that found in hydro-simulations. This is not too astonishing as it does not take into account that the Jeans length depends on temperature and density. Jeans smoothing at the mean temperature overestimates the smoothing in low density regions and underestimates it at higher density. This leads to significant differences of the flux statistics compared to hydro-simulations. Smoothing of the *evolved* dark matter density field on a global Jeans scale is therefore not a promising technique. The reason for the success of our FIT-1 and FIT-2 schemes is their adaptive nature which takes into account – at least to some extent – the density/temperature dependence of the Jeans scale.

We conclude that large high-resolution DM simulations combined with a two-parameter fit of the DM density gas density relation obtained from hydro-dynamical simulations are the best compromise between computational expense and accuracy when a large dynamic range and/or an extensive parameter study are required.

ACKNOWLEDGMENTS

We thank Lauro Moscardini, Francesco Miniati, Bepi Tormen, Joop Schaye and Simon White for useful discussions and technical help. MV acknowledges partial financial support from an EARA Marie Curie Fellowship under contract HPMT-CT-2000-00132. TT thanks PPARC for the award of an Advanced Fellowship. This research was conducted in collaboration with Cray/SGI, utilising the COSMOS super computer at the Department for Applied Mathematics and Theoretical Physics in Cambridge. This work was supported by the European Community Research and Training Network ‘The Physics of the Intergalactic Medium’.

APPENDIX A: SPH INTERPOLATION ALONG LOS

In this Appendix we describe the SPH computation of physical quantities along a given line of sight through the box. We follow the same procedure described in (Theuns *et al.* 1998). We divide the sight line into $N \sim 2^{10}$ bins of width Δ in distance x along the sight line. For a bin j at position $x(j)$ we compute the density and the density weighted temperature and velocity for

the gas and density and weighted velocity for the dark matter from:

$$\rho_X(j) = \sum_i \mathcal{W}_{ij} \quad (\text{A1})$$

$$(\rho v)_X(j) = \sum_i v_{X(i)} \mathcal{W}_{ij} \quad (\text{A2})$$

$$(\rho T)_X(j) = \sum_i T(i) \mathcal{W}_{ij}. \quad (\text{A3})$$

$X(i)$ is a label indicating the abundance of species X of particle i ($X = \text{H I}$; $X = \text{IGM}$ and $X = \text{DM}$ denotes neutral hydrogen, total gas and dark matter density, respectively).

Here, $\mathcal{W}_{ij} = mW(q_{ij})/h_i^3$ and m is the SPH particle mass which is the same for all SPH particles (but different for DM and gas particles). For W we use the M4 spline (Monaghan 1992) given by

$$\begin{aligned} W(q) &= \frac{1}{\pi} (1 + q^2 (-1.5 + 0.75q)) \text{ if } q \leq 1 \\ &= \frac{1}{\pi} (0.25 (2 - q)^3) \text{ if } 1 \leq q \leq 2 \\ &= 0 \text{ elsewhere.} \end{aligned} \quad (\text{A4})$$

We have defined:

$$q_{ij} = \frac{|\mathbf{x}(i) - \mathbf{x}(j)|}{h_i}, \quad (\text{A5})$$

where $\mathbf{x}(i)$ and h_i are the position and SPH-smoothing length of particle i . Note that h is defined in such a way that on average 32 particles are within $2h(i)$ from particle i . In this way, for each pixel along the LOS, we compute the contribution of all the particles which influence this region with a weight given by eq. (A4); this is the ‘scatter’ interpretation (see, for example, Hernquist & Katz 1989). For the computation of the spectra we label bins according to velocity and we adopt the procedure described in Section 3.

REFERENCES

- Aguirre A., Schaye J., Theuns T., 2002, preprint
- Bahcall J.N., Salpeter E.E., 1965, ApJ, 142, 1677
- Bardeen J.M., Bond J.R., Kaiser N., Szalay A.S., 1986, ApJ, 304, 15
- Bi H.G., 1993, ApJ, 405, 479
- Bi H.G., Börner G., Chu Y., 1992, A&A, 266, 1
- Bi H.G., Davidsen A.F., 1997, ApJ, 479, 523
- Bi H.G., Ge J., Fang L.-Z., 1995, ApJ, 452, 90
- Bryan G.L., Machacek M. E., 2000, ApJ, 534, 57
- Bryan G.L., Machacek M. E., Anninos P., Norman M.L., 1999, ApJ, 517, 13
- Cen R., Miralda-Escudé J., Ostriker J.P., Rauch M., 1994, ApJ, 437, L83
- Charlton J.C., Anninos P., Zhang Y., Norman M.L., 1997, ApJ, 485, 26
- Coles P., Jones B., 1991, MNRAS, 248, 1
- Coles P., Melott A.L., Shandarin S.F., 1993, MNRAS, 260, 765
- Couchman, H. M. P., Thomas, P. A., Pearce, F. R., 1995, ApJ 452, 797
- Croft R.A.C., Weinberg D.H., Katz N., Hernquist L., 1998, ApJ, 495, 44

- Croft R.A.C., Weinberg D.H., Pettini M., Hernquist L., Katz N., 1999, *ApJ*, 520, 1
- Croft R.A.C., Weinberg D.H., Bolte M., Burles S., Hernquist L., Katz N., Kirkman D., Tytler D., 2001, *ApJ*, submitted, astro-ph/0012324
- Dobrzycki A., Bechtold J., Scott J., Morita M., 2001, preprint, astro-ph/0111487
- Eke, V.R., Cole, S., Frenk C.S., 1996, *MNRAS*, 282, 263
- Efstathiou G., Schaye J., Theuns T., 2000, *Philosophical Transactions of the Royal Society, Series A*, Vol. 358, no. 1772, p. 2049
- Feng L.-L., Fang L.-Z., 2000, preprint astro-ph/0001348
- Gnedin N.Y., Hui L., 1996, *ApJ*, 472, L73
- Gnedin N.Y., Hui L., 1998, *MNRAS*, 296, 44
- Gnedin N.Y., Hamilton A.J.S., 2001, preprint, astro-ph/0111194
- Gunn J.E., Peterson B.A., 1965, *ApJ*, 142, 1633
- Hernquist L., Katz N., 1989, *ApJ*, 70, 419-446
- Hernquist L., Katz N., Weinberg D.H., Miralda-Escudé J., 1996, *ApJ*, 457, L51
- Hui L., 1999, *ApJ*, 516, 525
- Hui L., Gnedin N.Y., Zhang Y., 1997, *ApJ*, 486, 599
- Hui L., Stebbins A., Burles S., 1999, *ApJ*, 511, L5
- Hui L., Burles S., Seljak U., Rutledge R. E., Magnier E., Tytler D., 2000, preprint astro-ph/0005049
- Petitjean P., Mueket J.P., Kates R.R., 1995, *A&A*, 295, L9
- Kim T.-S., Cristiani S., D'Odorico S., 2001, *A&A*, 373, 757
- Lahav O., Lilje P.B., Primack J.R., Rees M.J., 1991 *MNRAS*, 251, 128
- Matarrese S., Mohayaee, R., 2002, *MNRAS*, 329, 37
- McDonald P., 2001, preprint, astro-ph/0108064
- McDonald P., Miralda-Escudé J., 1999, *ApJ*, 518, 24
- McDonald P., Miralda-Escudé J., Rauch M., Sargent W.L.W., Barlow A., Cen R., Ostriker J.P., 2000, *ApJ*, 543, 1
- Melott A.L., Pellman T.F., Shandarin S.F., 1993, *MNRAS*, 269, 626
- Meiksin A., 1994, *ApJ*, 431, 109
- Meiksin A., Bryan G., Machacek M., 2001, *MNRAS*, 327, 296
- Miralda-Escudé J., Rees M., 1994, *MNRAS*, 266, 343
- Miralda-Escudé J., Cen R., Ostriker J.P., Rauch M., 1996, *ApJ*, 471, 582
- Miralda-Escudé J. et al., 1997, to appear in *Proceedings of 13th IAP Colloquium: Structure and Evolution of the IGM from QSO absorption line systems*, eds. P. Petitjean, S. Charlot
- Narayanan V.K., Spergel D.N., Davé R., Ma C.P., 2000, *ApJ*, 543, 103
- Nusser A., 2000, *MNRAS*, 317, 902
- Nusser A., & Haehnelt M., 1999, *MNRAS*, 303, 179
- Nusser A., & Haehnelt M., 2000, *MNRAS*, 313, 364
- Petry C.E., Impey C.D., Katz N., Weinberg D.H., Hernquist L.E., 2001, preprint, astro-ph/0110450
- Pichon C., Vergely J.L., Rollinde E., Colombi S., Petitjean P., 2001, *MNRAS*, 326, 597
- Rauch M., 1998, *ARA&A*, 36, 267
- Rauch M., Miralda-Escudé J., Sargent W. L. W., Barlow T. A., Weinberg D. H., Hernquist L., Katz N., Cen R., Ostriker J. P., 1997, *ApJ*, 489, 7
- Reisenegger A., Miralda-Escudé J., 1995, *ApJ*, 449, 476
- Ricotti M., Gnedin N. Y., Shull, J.M., 2000, *ApJ*, 534, 41
- Roy Choudhury T., Padmanabhan T., Srianand R., 2001, *MNRAS*, 322, 561
- Roy Choudhury T., Srianand R., Padmanabhan T., 2001, *ApJ*, 559, 29
- Sathyaprakash B.S., Sahni V., Munshi D., Pogosyan D., Melott A.L., 1995, *MNRAS*, 275, 463
- Schaye J., Theuns T., Rauch M., Efstathiou G., Sargent W.L.W., 2000, *MNRAS*, 318, 817
- Seljak U., Zaldarriaga M., 1996, *ApJ*, 469, 437
- Schaye J., 2001, *ApJ*, 559, 507
- Sugiyama N., 1995, *ApJS*, 100, 281
- Theuns T., Schaye J., Haehnelt M.G., 2000, *MNRAS*, 315, 600
- Theuns T., Leonard A., Efstathiou G., Pearce F.R., Thomas P.A., 1998, *MNRAS*, 301, 478
- Theuns T., Zaroubi S., Kim T.-S., Tzanavaris P., Carswell R.F., 2001, astro-ph/0110600
- Viel M., Matarrese S., Mo H.J., Haehnelt M.G., Theuns T., 2002, *MNRAS*, 329, 848
- White M., Croft R.A.C., 2000, *ApJ*, 539, 497
- Zaldarriaga M., Scoccimarro R., Hui L., 2001, preprint, astro-ph/0111230
- Zel'dovich Ya. B., 1970, *A&A*, 5, 84
- Zhang Y., Anninos P., Norman M.L., 1995, *ApJ*, 453, L57
- Zhang Y., Anninos P., Norman M.L., Meiksin A., 1997, *ApJ*, 485, 496
- Zhang Y., Meiksin A., Anninos P., Norman M.L., 1998, *ApJ*, 495, 63